

LOAN DOCUMENT

DTIC ACCESSION NUMBER	PHOTOGRAPH THIS SHEET	INVENTORY																
	LEVEL																	
	<p><i>Low Background VL WIR SCA</i> <i>Characterization for the David Program</i></p> <p>DOCUMENT IDENTIFICATION 2000</p>																	
<p>DISTRIBUTION STATEMENT A Approved for Public Release Distribution Unlimited</p>																		
DISTRIBUTION STATEMENT																		
<p>ACCESSION FOR</p> <table border="1"><tr><td>NTIS</td><td>GRAM</td><td><input checked="" type="checkbox"/></td></tr><tr><td>DTIC</td><td>TRAC</td><td><input type="checkbox"/></td></tr><tr><td>UNANNOUNCED</td><td></td><td><input type="checkbox"/></td></tr><tr><td>JUSTIFICATION</td><td></td><td></td></tr></table> <p>BY</p> <p>DISTRIBUTION/</p> <p>AVAILABILITY CODES</p> <table border="1"><tr><td>DISTRIBUTION</td><td>AVAILABILITY AND/OR SPECIAL</td></tr><tr><td>A-1</td><td></td></tr></table>			NTIS	GRAM	<input checked="" type="checkbox"/>	DTIC	TRAC	<input type="checkbox"/>	UNANNOUNCED		<input type="checkbox"/>	JUSTIFICATION			DISTRIBUTION	AVAILABILITY AND/OR SPECIAL	A-1	
NTIS	GRAM	<input checked="" type="checkbox"/>																
DTIC	TRAC	<input type="checkbox"/>																
UNANNOUNCED		<input type="checkbox"/>																
JUSTIFICATION																		
DISTRIBUTION	AVAILABILITY AND/OR SPECIAL																	
A-1																		
DATE RECEIVED IN DTIC																		
REGISTERED OR CERTIFIED NUMBER																		
DATE RETURNED																		
DATE ACCESSIONED																		
DISTRIBUTION STAMP																		

H
A
N
D
L
E

W
I
T
H

C
A
R
E

LOW BACKGROUND VLWIR SCA CHARACTERIZATION FOR THE DAVID PROGRAM

By

Eugene McLean, Raytheon Infrared Operations
Rodolfo Ramos, Air Force Research Labs
John Hubbs, Ball Aerospace & Technology Corp.
Le Pham, Raytheon Infrared Operations
Bruce Bozovich, Raytheon Infrared Operations
Dave Rhiger, Raytheon Infrared Operations

Abstract

The Development of Advanced Very Long Wavelength Infrared Detectors (DAVID) Program, managed by the Air Force Research Laboratory (AFRL), is designed to advance the development of focal plane arrays for applications in space-based surveillance. In order to achieve the requirements for very long wavelengths and high sensitivities, extremely challenging demands are placed on the both the detector material and the readout integrated circuit (ROIC) technology. To produce exceptionally low detector leakage currents, for instance, detector developments with low doping and advanced molecular beam epitaxy (MBE) growth techniques have been evaluated. Also needed were ROICs with low noise performance as well as capability for accommodating a wide variation in detector characteristics including R_0A , back bias, and $1/f$ noise. This paper will discuss and compare these focal plane requirements with the program results achieved to date. Current data, including the NEI, will demonstrate that focal planes with BLIP limited performance can be achieved even with backgrounds in the 10^{12} photons/cm/sec range.

1.0 INTRODUCTION

The Development of Advanced Very Long Wavelength Infrared Detectors (DAVID) is being carried out by Raytheon Infrared Operations (RIO), under contract to the Air Force with BMDO funding. This three-year technology development directly supports the focal plane requirements of SBIRS-Low. On this program, RIO has fabricated and tested Sensor Chip Assemblies (SCAs) against specifications corresponding to strategic VLWIR applications. This paper gives an overview of the DAVID program, with goals and

objectives, the HgCdTe device structure, and the architecture of the SCA described. In addition, key test results of individual detectors are presented, and the SCA test results are reviewed.

2.0 PROGRAM OVERVIEW AND GOALS

The DAVID Program was established to develop the technology for future VLWIR focal plane requirements of the Space-Based Infrared System-Low-altitude (SBIRS-Low), designed to acquire missiles during launch, and then to track the vehicle, payloads, and decoys in mid-course after rocket burnout. Because these objects are relatively small and can have reduced temperatures, it is a tremendous challenge to detect and track them from long ranges. The potentially low temperature of the targets favors LWIR and VLWIR spectral bands. However, the cold body tracking application places unusual demands on detector performance. The specific DAVID challenge is to improve the performance and uniformity of HgCdTe focal planes in order to satisfy these critical system requirements.

The DAVID Program is the successor to the very successful LLUM program at Raytheon, which demonstrated SCAs operating with a 12 μ m cutoff at 40 K, having D^* values of 10^{14} Jones with operability of 99% in background flux levels of only 10^{11} photons $\text{cm}^{-2} \text{sec}^{-1}$. It was subsequently decided that, in order to meet the needs of SBIRS-Low, the DAVID Program should extend the wavelength sensitivity out to a 14 μ m cutoff, while maintaining the operating temperature at 40 K.

The specific goals of DAVID are:

- (1) extend the spectral response of HgCdTe to 14 μ m,
- (2) achieve the same D^* and NEI as LLUM,
- (3) maintain the operating temperature at 40 K, and
- (4) meet the stated radiation hardness requirements.

The DAVID program performance requirements are summarized in Table 1. Note that these specifications are quite similar to those for the previous LLUM program, except for the cut-off wavelength, which has been extended to 14 μ m.

*Approved for Public Release;
Distribution is Unlimited.*

Table 1. Summary of DAVID Program Requirements

Parameter	Value
Format	128 x 128
Pixel Size	60 μm x 60 μm
Cut-off Wavelength	14.0 μm
Operating Temperature	40 Kelvin
Integration Time	X ms
Noise Equivalent Input (NEI) at $E_a = 5 \times 10^{10}$ ph/sec-cm ²	X photons/sample
Total Dose Hardness Level	X krad(Si)
Instantaneous Dynamic Range	1000
Photon Irradiance Operational Range (ph/sec-cm ²)	$10^{11} - 10^{14}$
Operability	>95%

RIO's approach has been to make improvements in material quality and device design, and to run recurring lots in order to assess the improvements. A very important technical issue has been the leakage current in the p-n junction of the detector. Because detector noise scales with this current, we have focused on material improvements that would lead to reduced leakage. Because of the 40 K operating temperature, unlike tactical LWIR focal planes, the dominant mechanism of current at the junction is not diffusion but defect-related leakage. Hence, attention to material quality has been a critical focus of the DAVID program.

3.0 MATERIAL AND DEVICES

3.1 HgCdTe Detector

The detector structure for DAVID is the same as that used in numerous production programs at Raytheon, but with more stringent specifications applied to the material because of the demanding performance requirements. Figure 1 shows a cross-section diagram of the detector unit cell. The structure starts with the bulk-grown CdZnTe substrate. Two layers are then grown by liquid phase epitaxy (LPE) from Hg melts. The first is the n-type VLWIR base layer, in which the photons are absorbed; the second is the p-type cap layer. An etching process forms the mesas and delineates the pixels. To complete the structure, the CdTe surface passivation, the metal contact, and the

indium bump are applied in sequence. The wafer is then diced into detector arrays. After dicing, individual arrays are hybridized to Si readout integrated circuit (ROIC) chips to form the SCAs. On the same wafer, some test structure arrays are fabricated simultaneously with the main arrays. The test structures are hybridized to fanouts allowing detailed testing to be performed on individual diodes.

Figure 2 shows a scanning electron microscope view of a mini array in a test structure. This has the same geometry as the main DAVID array with 60 μm square unit cell. The photo shows the completed unit cell just prior to hybridization, with passivation, contact metal, and indium bump in place. This configuration has been utilized to build more than 10,000 deliverable HgCdTe detector assemblies and has been adapted to the needs of the VLWIR requirements of the DAVID Program. The architecture allows an indium bump to be used for both mechanical and electrical interface with the detector on a per pixel basis, allowing the detector to interface to a low noise amplifier immediately adjacent to the detector.

Before the main arrays are hybridized, each wafer is evaluated by means of automated probing of the wafer at 78 K (prior to dicing), and by subsequent dewar testing of the hybridized test structures at 78 and 40 K. Many of the wafers, belonging to Lots 1A through 3A, have shown excellent R_0A values, as illustrated

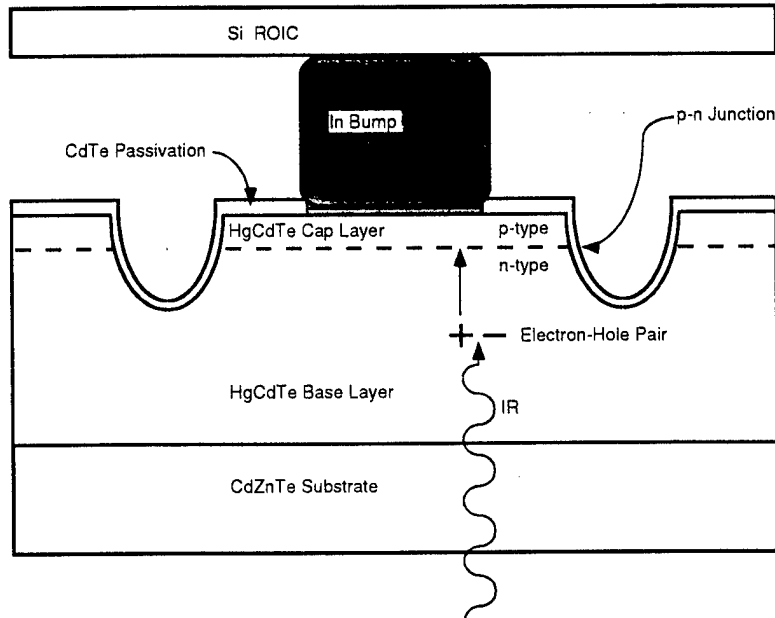


Figure 1. HgCdTe Unit Cell and Hybridized ROIC

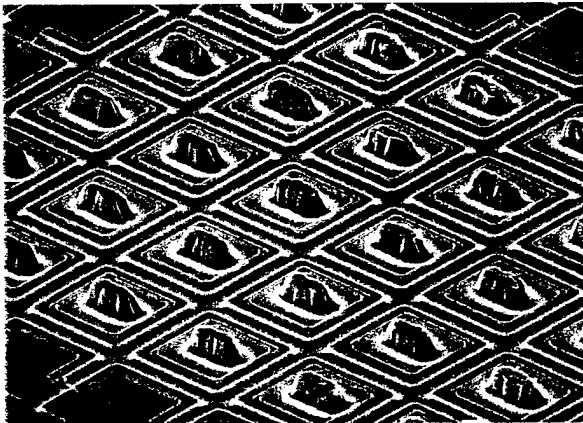


Figure 2. SEM Photo of Detector Array Prior to Hybridization

in Figure 3. Each data point in Figure 3(a) represents the median value of R_0A for a full wafer, as measured on diodes that have been included for the purpose of autoprobing. The area used here is the junction area, which is $50 \mu\text{m}^2$. Many of the wafers lie at or above the curve, which is the diffusion-limited trendline. Figure 3(b) shows very good results at 40 K. These points represent median values of RA for a test structure from each wafer. The data were obtained in zero field of view on the mini-array composed of $60 \mu\text{m}$ pixels. The junction area is $50 \mu\text{m}^2$, but the $60 \mu\text{m}$ optical area

is used to calculate RA. The solid symbols indicate R_0A (at zero bias), while the open symbols indicate R_0A at 20 mV reverse bias. At this temperature the leakage current originates with generation effects or trap-assisted tunneling. The values in Figure 3(b) are generally very good with respect to the trendline.

3.2 Readout ROIC

The readout design is based on an auto-zeroed capacitance transimpedance amplifier (CTIA) unit cell amplifier. The signal chain is shown in Figure 4. The non-adjustable detector bias is provided by an auto-zero capacitor that is reset once per frame time and sets the detector bias to approximately -10 mVolts . This ac coupling to the detector bias node mitigates the effects of radiation induced circuit threshold shifts on the detector bias. Additional readout design features include on-chip correlated double sampling, sample and hold amplifiers, and push-pull output amplifiers. The readouts were fabricated at the Raytheon Micro Electronics Division (MED) using an isoplanar cryogenic CMOS process together with a re-oxidized oxy-nitride (RONO) gate dielectric. This process was used to enhance the total dose radiation hardness of the DAVID focal plane arrays that is required for space applications.

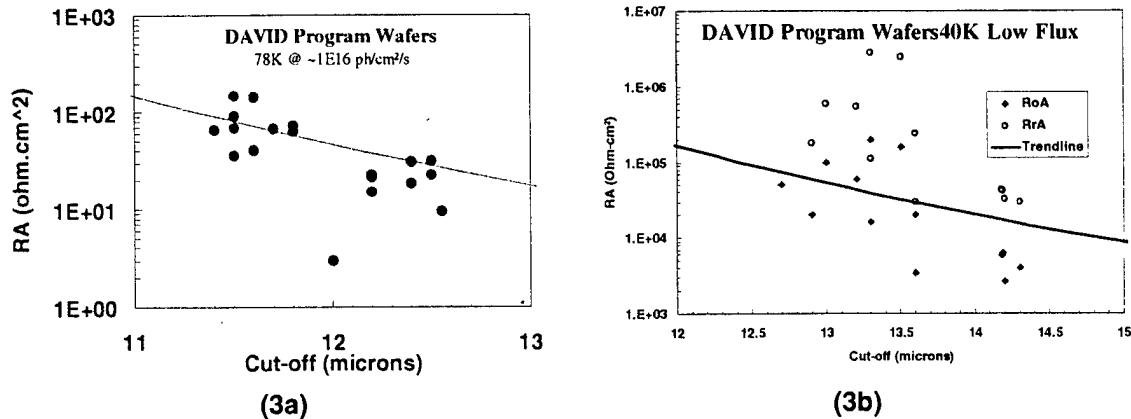


Figure 3. R_oA versus cutoff wavelength for diodes of the DAVID program, at (a) 78 K and at (b) 40 K. Three lots are combined in each plot.

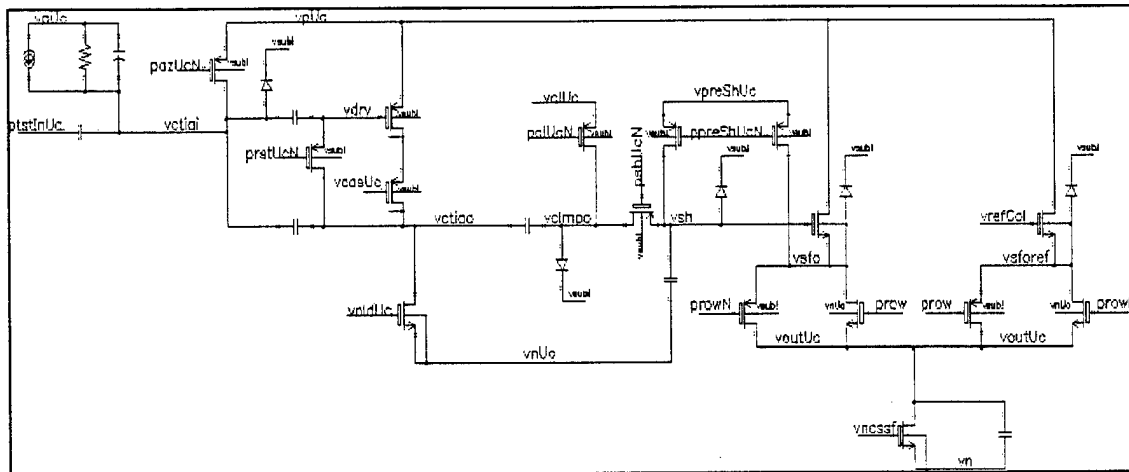


Figure 4. Signal Chain for Raytheon DAVID Readout.

4.0 SCA Results

4.1 Introduction

Raytheon fabricated three recurring lots of wafers and evaluated each wafer in terms of the test structures described above. From this evaluation, main arrays were selected for hybridization to ROICs. After hybridization, the SCAs were given an initial screen testing; if they passed the basic functionality screen, then they went on for further radiometric tests. The best resulting SCAs were then tested at Raytheon and Ball Aerospace, using the test facility diagrammed in Figure 5. The test conditions were designed to duplicate the anticipated systems application for the DAVID Program. The devices were typically evaluated at two different backgrounds, which allowed assessment of the SCA performance across a wide range of operating conditions. The

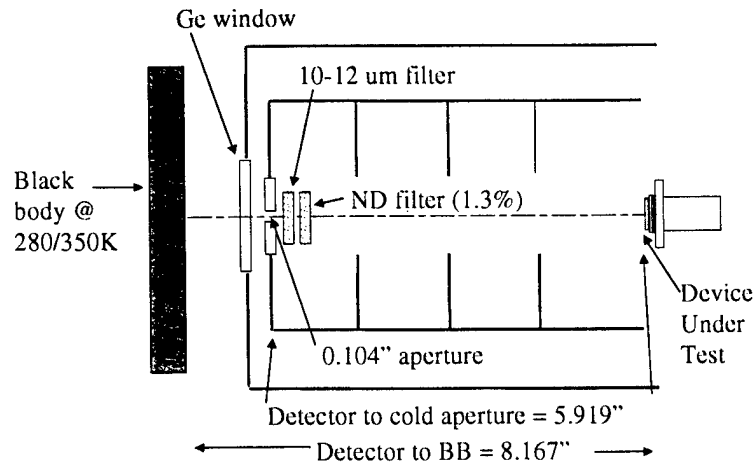
test backgrounds were: $2-5 \times 10^{11}$ ph/cm²-s and $2-5 \times 10^9$ ph/cm²-s.

4.2 Test Data

This paper will report on the better devices that were fabricated and tested in DAVID Lots 1 and 2. In Figure 6, the data demonstrate that several SCAs had excellent performance, with NEI below 4000. The implications of improving the lower performing devices will be discussed at the end of this paper.

The calculated NEI and D^* , based on the measured median noise and responsivity at 10.8 μ m for a Lot 1 device, are shown in Figure 7. Included with the measured data are plots of the Background Limited Performance (BLIP) NEI and D^* for a detector quantum efficiency of 51%. The deviation from BLIP performance, evident at irradiances below approximately 3×10^{11}

UNCLASSIFIED



Temperature ==> 40K-60 K

High background flux 280/350 ==> $2.13 \times 10^{11} / 5.58 \times 10^{11} \text{ ph/cm}^2\text{-s}$

Low background flux 280/350 ==> $2.26 \times 10^9 / 5.91 \times 10^9 \text{ ph/cm}^2\text{-s}$

f # ==> ~60

Aperture diameters (hi/lo Qb) ==> 0.104" / 0.0107"

Integration times ==> normally 10ms, but 2ms and 5ms available

Figure 5. Typical Test Conditions for the SCA Evaluations

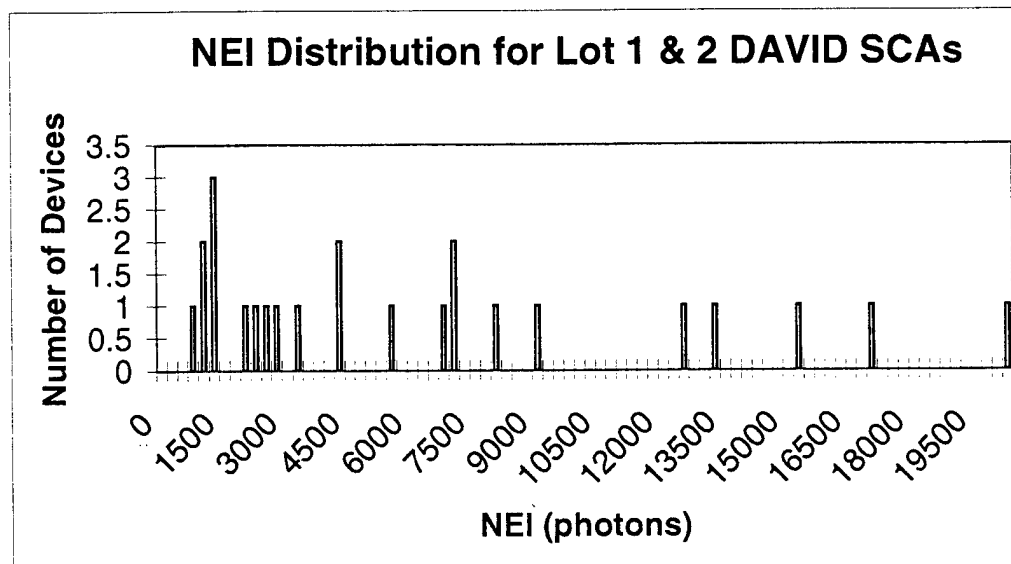


Figure 6. Distribution of all measured NEIs for the Lot 1 and Lot 2 data

UNCLASSIFIED

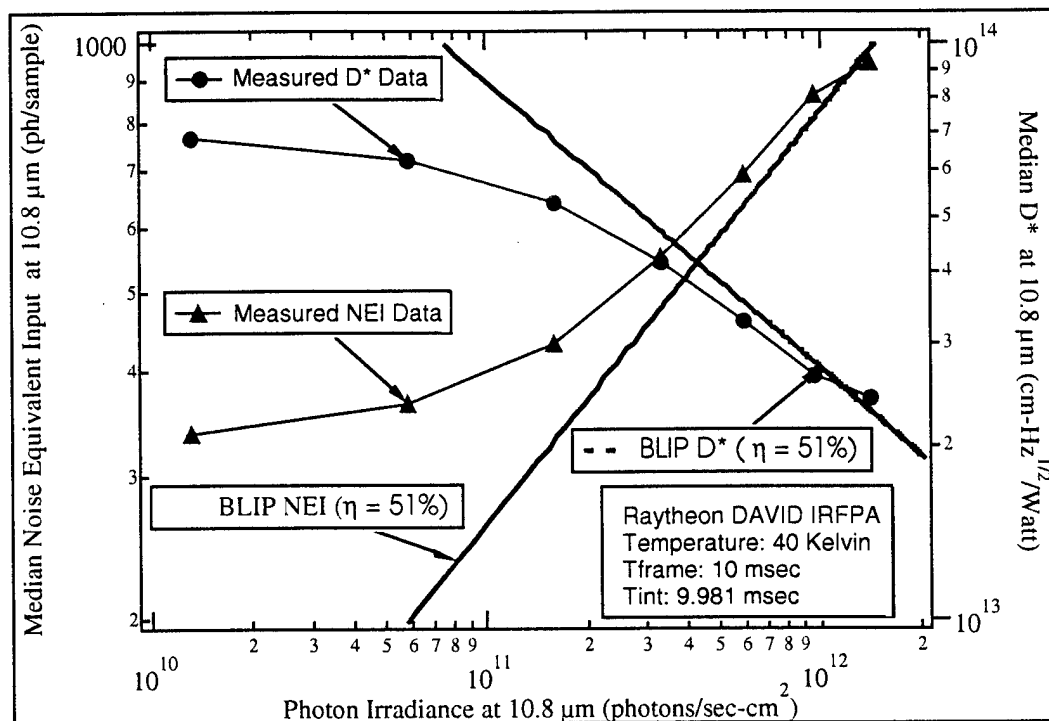


Figure 7. Median NEI and D* versus Photon Irradiance for Lot 1 device

photons/sec-cm², is due to the domination of detector thermal and 1/f noise. These data again demonstrate the performance enhancements that could be obtained by further reducing the detector thermal and 1/f noise.

The Lot 1 data shown in Figure 8 were taken two years ago and represented the state of the art for VLWIR material at the time. The RoA distribution is centered on 2×10^5 , which is excellent for the measured 13.5 μm cutoff material.

Later Lot 2 devices demonstrated even better performance levels. In Figure 9, the responsivity of a Lot 2 device shows a classical Gaussian distribution with a one sigma value of 2.8%; this is an exceptionally well behaved signal distribution for a 12.8TBR μm device.

Figure 10 shows the noise equivalent irradiance for two different backgrounds: 1.3×10^{10} and on 2.1×10^{12} . These distributions demonstrate largely classical behavior with, respectively, 35% and 14% non-uniformity for most pixels. The average NEI as a function of photon irradiance, in Figure 11, shows that it is photon limited at backgrounds above 3×10^{11} . Although the device performance is significantly

better than requirements, the data indicates that read noise dominates the low background performance. Since this result was unexpected, we have proposed some alternative clamp timing that is anticipated to improve the read noise.

Table 2 compares test results of two selected SCAs representing Lots 1 and 2, respectively. A distinct improvement in detector performance is evident in Lot 2. The quantum efficiency η has been raised from 51% to 60%, while the dark current has been lowered. The RA (measured at approximately -10 mV) has been significantly increased, and the responsivity uniformity, going from 6.8% down to 2.6%, has been improved substantially. In addition to the improvements made in detector fabrication, there was a modification of the ROIC design, which greatly increased the dynamic range. This is evident in the output voltage swing, the well capacity, and the maximum allowed irradiance level at full integration time, as listed in Table 2. Output voltage swing, for example, has been increased from 0.7 V to more than 2.5 V. At the same time, however, the modification of the readout has resulted in an increase in read noise

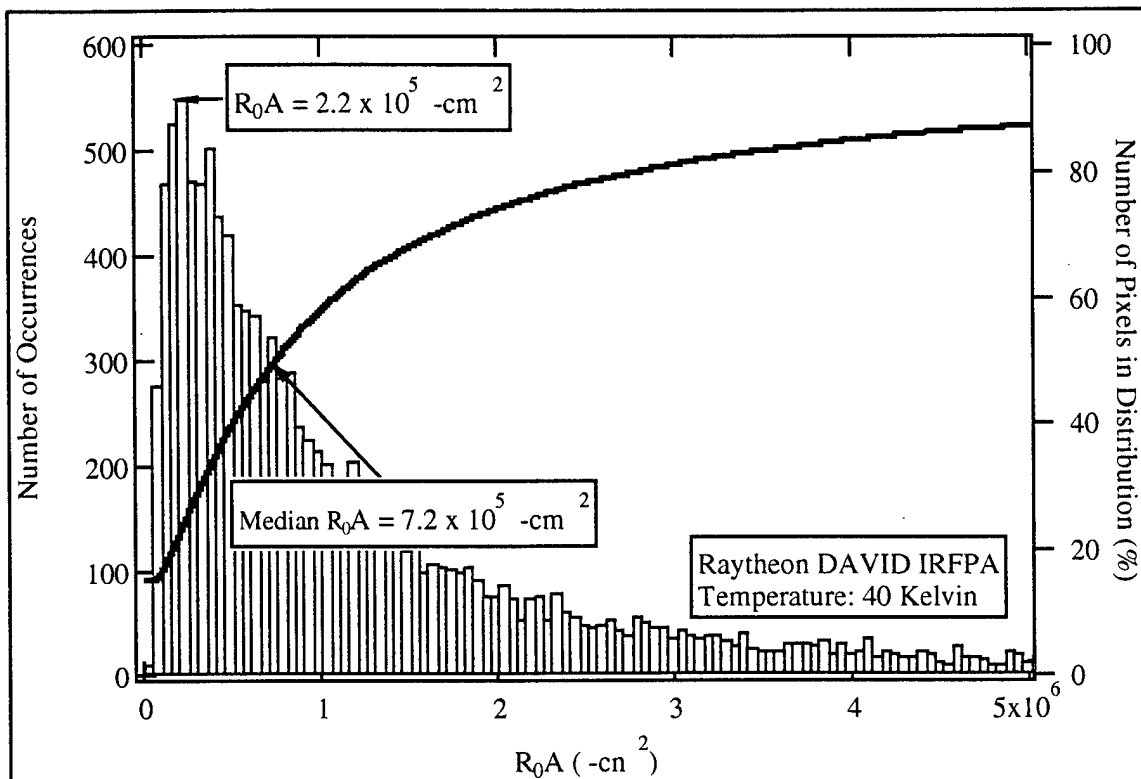


Figure 8. Distribution of RoA products for the entire distribution of pixel element

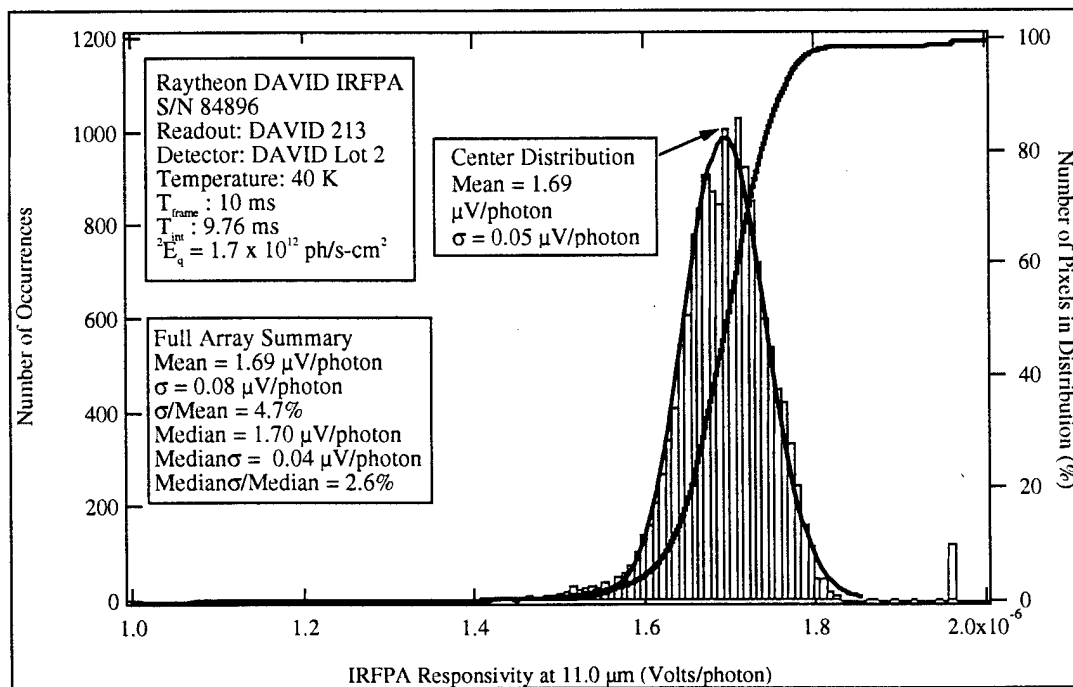


Figure 9. Signal Histogram for Lot 2 device showing Gaussian distribution

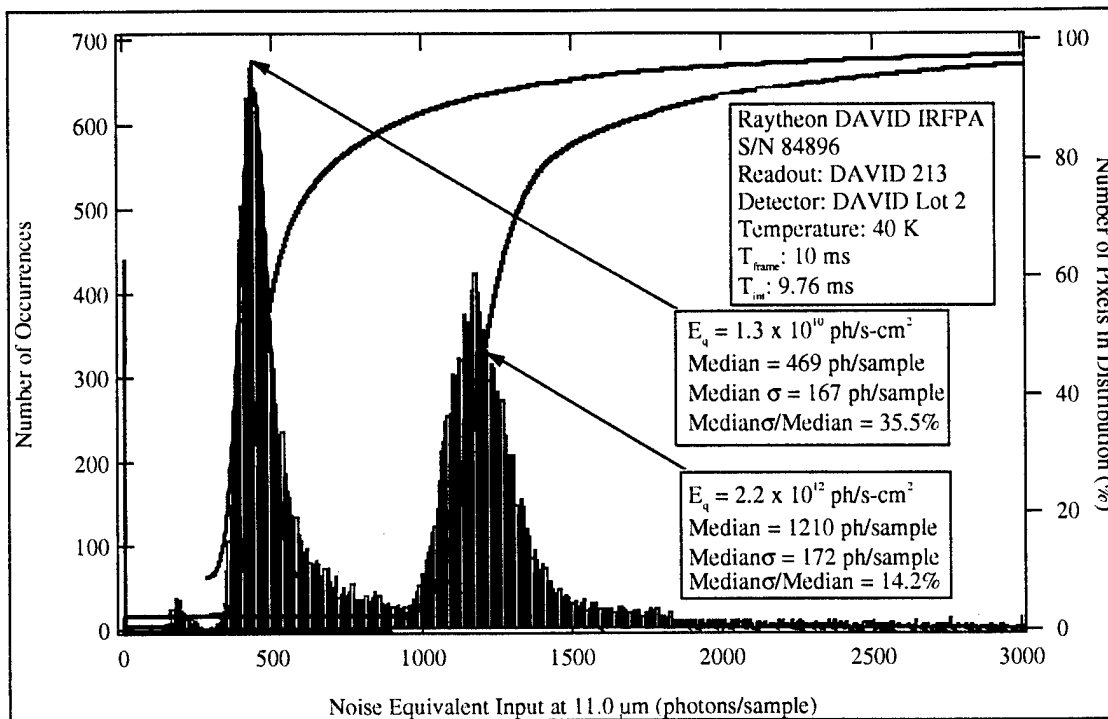


Figure 10. NEI distributions for two different backgrounds for Lot 2 device

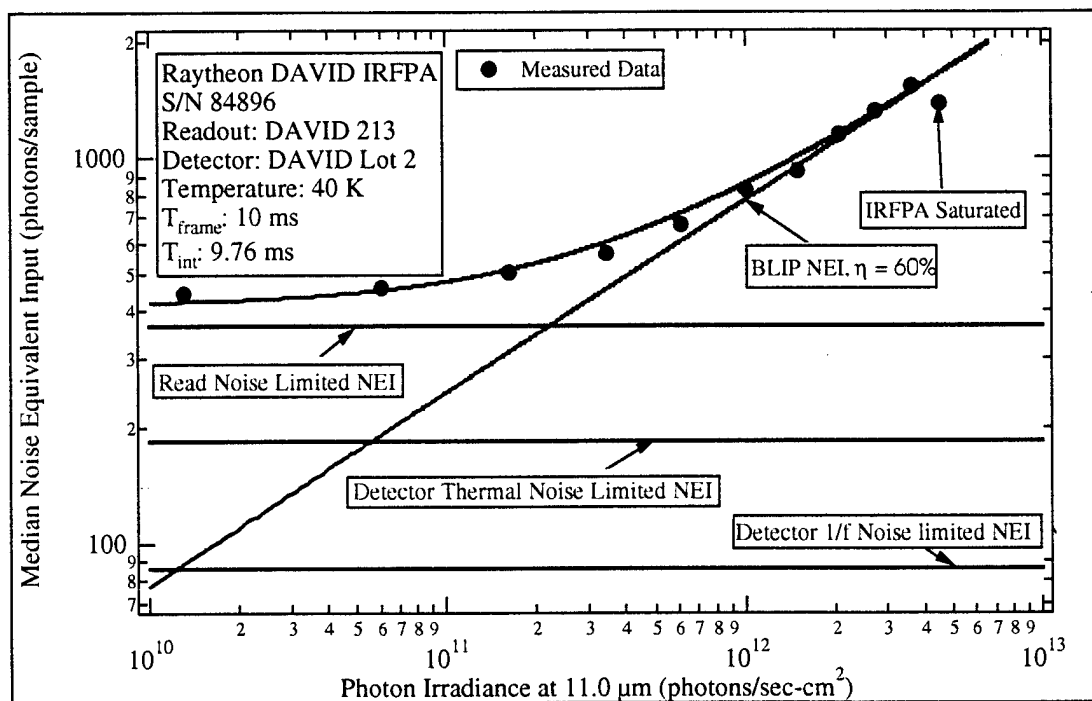


Figure 11. Noise Equivalent Irradiance (NEI) as a function of background

Table 2. Summary of test results at 40 K for SCAs representing Lot 1 and Lot 2.

Parameter	Sensor Chip Assembly S/N: 70689	Sensor Chip Assembly S/N: 84896
Detector Lot	Lot 1	Lot 2
Readout Design	SBRC184	SBRC213
η at 11.0 μm	51 %	60 %
I_{dark} at 40 K	0.26 pA	0.17 pA
Median RA	$7 \times 10^5 \text{ ohm cm}^2$	$2 \times 10^6 \text{ ohm cm}^2$
NEI at $E_q = 1.0 \times 10^{10} \text{ ph/s-cm}^2$	330 ph/sample	450 ph/sample
NEI at $E_q = 1.0 \times 10^{12} \text{ ph/s-cm}^2$	850 ph/sample	875 ph/sample
Responsivity Uniformity (σ / mean)	6.8 %	2.6 %
Read Noise	225 μV	700 μV
Conversion Gain (Transimpedance)	2.6 $\mu\text{V/el}$	3.0 $\mu\text{V/el}$
Output Voltage Swing	0.7 V	> 2.5 V
Well Capacity	270,000	>850,000
Max Irradiance Level at Full Integration Time	$1.0 \times 10^{12} \text{ ph/s-cm}^2$	$4.0 \times 10^{12} \text{ ph/s-cm}^2$
Power Dissipation	~20 mW	~100 mW
Cutoff Wavelength (per watt)	13.2 μm	13.5 μm

from 225 to 700 μV . As a consequence, the NEI (noise equivalent irradiance) in Table 2 at the lower background flux has increased from 330 to 450 photons/sample going from Lot 1 to Lot 2. For the former, it is dominated by detector noise; but for the latter, the readout noise is dominant. This is why we are evaluating the source of the read noise to assess whether a clocking change can substantially lower the noise. In contrast, the NEI in Table 2 at the higher background level is about the same for both lots (850 and 875 photons/sample) because here the detector is operating in the background-limited (BLIP) regime.

In Figure 12, the RoA distribution of all pixels at 40K shows the average of 2.3×10^6 . Although this is excellent performance for a VLWIR cutoff of 13.5 microns, there are still a large percentage of diodes significantly lower than 2 to 3×10^6 . These diodes also produce the long tail in the NEI plots shown in Figure 10.

From a detector development point of view, the long tail in the population distribution at higher

NEI indicates that there is a significant number of leaky diodes. These diodes have a higher current that is manifested as higher noise. The principal reason for this tail is the leakage current itself. Another contributing factor is the $1/f$ noise, but empirically it is known to scale with leakage. In order to minimize the leakage current, we are working on a variety of approaches. The first is to lower the doping in the n-type base layer. The benefits will be an increase in the carrier lifetime and a decrease in the electric field within the depletion region. The lower field will substantially reduce tunneling currents, which can dominate at 40 K. Also, we are working on methods to remove from the material the impurities that could form trap sites that facilitate leakage. Another approach has been to reduce the area of the p-n junction, because several leakage mechanisms should be proportional to area. All of these efforts may lead to lower leakage, and greater uniformity of the NEI distribution. Lowered base layer doping is a main thrust of the next lot.

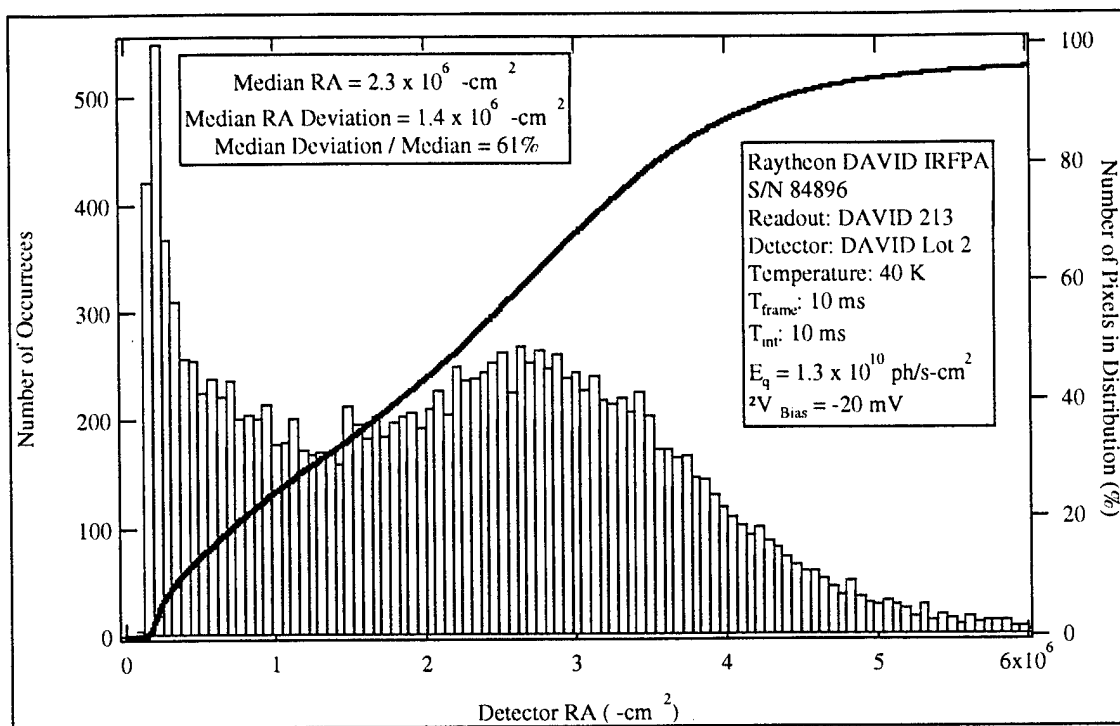


Figure 12. RoA pixel distribution of Lot 2 device

5.0 SUMMARY AND CONCLUSIONS

The DAVID Program is developing VLWIR diode technology for low background applications such as SBIRS-Low. Fundamental material properties as well as array fabrication techniques are being addressed to improve the low temperature leakage performance of these diodes. Results of test structures hybridized to diode arrays showing high performance diodes at the 12-14 micron range have been demonstrated. These diode arrays have been hybridized to low noise ROICs and the resulting SCAs have been characterized. Raytheon's DAVID devices have demonstrated NEIs of less than 500 noise

electrons at 2×10^9 backgrounds. Although there are still issues with respect to the lowest performing 5 to 10 percent of the diodes, a development program involving improved detector structures, lower doped materials, and improved materials purity has been outlined to address these lower performing diodes.

Raytheon's DAVID results, thus far showing substantial progress between Lot 1 SCAs and Lot 2 SCAs, provide confidence that this technology can produce the uniform, low noise, high signal devices required for future strategic applications.